Submitted: 24 November, 2024 Accepted: 27 December, 2024 Published: 15 May, 2025 DOI:10.22514/ejgo.2025.061

ORIGINAL RESEARCH

European Journal of Gynaecological Oncology

Functional, microarray and bioinformatics analyses of human papillomavirus E7-specific pathways in cervical carcinogenesis

Nan Qi[1], Takeo Minaguchi[2,*], Kaoru Fujieda[2], Asami Suto[2], Hiroya Itagaki[2], Yuri Tenjimbayashi[2], Ayumi Shikama[2], Nobutaka Tasaka[2], Azusa Akiyama[2], Sari Nakao[2], Toyomi Satoh[2]

[1]Doctoral Program in Obstetrics and Gynecology, Graduate School of Comprehensive Human Sciences, University of Tsukuba, 305-8577 Tsukuba, Japan
[2]Department of Obstetrics and Gynecology, Institute of Medicine, University of Tsukuba, 305-8575 Tsukuba, Japan

***Correspondence**
minaguchit@md.tsukuba.ac.jp
(Takeo Minaguchi)

Abstract

Background: Human papillomavirus (HPV) vaccines are still ineffective for already infected patients. The development of new prophylactics and therapeutics for cervical cancer is hence urgently required particularly for contries and regions where medical resources are lacking. The mRNAs encoding the HPV oncogenes *E6* and *E7* are bicistronic and generated from the same pre-mRNA. Alternative splicing produces different mRNA variants, with the resultant balance of E6/E7 levels impacting downstream functions. Accumulating evidence suggests that E7 may contribute more closely to cervical carcinogenesis than E6. The aim of this study was to explore the E7-specific carcinogenic pathways. **Methods**: Small interfering RNAs knocking down either E6 or E6/E7 were transfected into CaSki and HeLa cells, and the analyses of cellular effects, microarray and bioinformatics were conducted. The survival of patients with cervical cancer based on gene expressions was analyzed utilizing a web database tool. **Results**: E7 knockdown induced G_1 cell cycle arrest and inhibited cellular proliferation, clonogenicity and transformation. Microarray analyses identified 15 E7-specific differentially expressed genes (DEGs), and their functional annotations included "epithelial-to-mesenchymal transition", "chromatin remodeling", "focal adhesion: phosphatidylinositol 3-kinase (PI3K)-AKT serine/threonine kinase (Akt)-mammalian target of rapamycin (mTOR)-signaling pathway" and "DNA-binding transcription factor activity". Pathway interaction analysis revealed that G_1 cell cycle arrest was the most significant and pivotal pathway. Among the E7-specific DEGs, aldo-keto reductase family 1 member B10 (*AKR1B10*), family with sequence similarity 78 member A (*FAM78A*) and AHNAK nucleoprotein 2 (*AHNAK2*) exhibited tumor-suppressive effects, whereas forkhead box A1 (*FOXA1*), SMAD family member 9 (*SMAD9*) and plastin 1 (*PLS1*) showed oncogenic effects in survival analysis, being consistent with the expression fold differences by the microarray. **Conclusions**: The identified DEGs were suggested to be involved in E7-specific cervical carcinogenesis by cooperating via multiple mechanisms, providing potential novel targets and biomarkers for the more efficient prevention and treatment of cervical cancer.

Keywords

Human papillomavirus; E6; E7; Cervical cancer; Microarray; Bioinformatics

1. Introduction

A total of 348,874 women died from cervical cancer and the age-standardized mortality rate was 7.1 in 2022 worldwide (https://gco.iarc.fr/today/home). At present, cervical cancer is the fourth most common cancer and the fourth leading cause of cancer death in women (https://gco.iarc.fr/today/home). The major causative factor for the development of cervical cancer is human papillomavirus (HPV) infection [1]. Although prophylactic HPV vaccines have been shown to reduce cervical cancer risk, they are still ineffective for already infected patients. It is urgently necessary to develop new prophylactics and therapeutics particularly for countries and regions where medical resources are lacking.

HPV has a round virion containing 8-Kb circular double-stranded DNA. The HPV genome contains the six early genes, *E1*, *E2*, *E4*, *E5*, *E6* and *E7*, as well as the two late genes, *L1* and *L2*, which encode capsid proteins [2]. *E6* and *E7* encode the oncoproteins, which serve pivotal roles in cervical carcinogenesis by degrading and inactivating the tumor suppressors p53

and Rb, respectively [2]. The major downstream functions of p53 include apoptosis [3], while those of Rb include G_1 cell cycle arrest [4]. In addition to these, E6 and E7 mediate a diverse range of other oncogenic pathways [5, 6]. To date, >200 types of HPV have been identified based on the sequence of the L1 gene. High-risk HPVs (HR-HPVs) include types 16, 18, 31, 33, 35, 39, 45, 51, 52, 56, 58, 59, 68, 73 and 82 [7], and are responsible for >99.7% of cervical cancers [8]. Among HR-HPVs, HPV16 and 18 are the most prevalent types; 55% of cervical cancers are HPV16-positive and 15% are HPV18-positive [8].

The mRNAs encoding E6 and E7 are bicistronic and are generated from the same pre-mRNA [9]. E6 is mainly translated from unspliced mRNA, and E7 is translated from spliced mRNAs [9]. Alternative splicing produces different mRNA variants, and the resultant balance of E6/E7 protein levels impacts downstream cellular effects [9]. Accumulating evidence [10–13], including our previous study [14], suggests that E7 may contribute more closely to cervical oncogenesis than E6. Therefore, targeting the E7-specific carcinogenic pathway is thought to provide more efficient prophylactic and therapeutic potentials for cervical cancer. However, the underlying molecular mechanisms are not yet fully clarified. The present study explored the E7-specific pathways of cervical carcinogenesis by utilizing microarray and bioinformatics analyses in HeLa and CaSki human cervical cancer cells, in which E6 or E6/E7 was knocked down. The present findings have significant implications for understanding detailed molecular mechanisms of cervical carcinogenesis, as well as for developing more efficient novel prophylactics and therapeutics for cervical cancer.

2. Materials and methods

2.1 Cell lines and culture

CaSki (HPV16-positive) and HeLa (HPV18-positive) cell lines were purchased from American Type Culture Collection. Cells were maintained in Dulbecco's Modified Eagle Medium (Nissui Pharmaceutical Co., Ltd., Tokyo, Japan, 05915) containing 10% fetal bovine serum (Gibco; Thermo Fisher Scientific, Inc., Grand Island, NY, USA, 10437-028) and 1 U/mL penicillin-streptomycin-amphotericin B suspension (FUJIFILM Wako Pure Chemical Corporation, Osaka, Japan, 161-23181) at 37 °C with 5% CO_2.

2.2 Small interfering RNA (siRNA)

A total of 3×10^5 cells were seeded in 60-mm dishes in antibiotics-free medium and cultured overnight. Cells were transfected with siRNAs at a concentration of 10 nM (HeLa cells) or 40 nM (CaSki cells) using Lipofectamine RNAiMAX (Thermo Fisher Scientific, Inc., Tokyo, Japan, 13778-150) following the manufacturer's instructions. The siRNAs (16E6E7, 16E6, 18E6 and 18E6E7) were synthesized by GE Healthcare Dharmacon, Inc. (Tokyo, Japan), and their targets and sequences are described in Table 1 (Ref. [15]). The siRNA sequences were subjected to National Center for Biotechnology Information (NCBI)-Nucleotide Basic Local Alignment Search Tool (BLASTN) for similarity against the human Reference Sequence (RefSeq) RNA database with no significant matches identified (https://blast.ncbi.nlm.nih.gov/Blast.cgi). In principle, the full-length mRNA encodes the E6 protein, and the spliced short mRNAs encode the E7 protein [9]. siRNAs 16E6 and 18E6 are designed to target the spliced-out region of mRNA, and siRNAs 16E6E7 and 18E6E7 are designed at the non-spliced-out region of mRNA. Accordingly, 16E6 and 18E6 inhibit only the full-length mRNA, thereby knocking down only the E6 protein, and 16E6E7 and 18E6E7 inhibit both the full-length and the spliced mRNAs, thereby knocking down both the E6 and E7 proteins [15] (Table 1). Non-specific (NS) siRNA was purchased from GE Healthcare Dharmacon, Inc (Tokyo, Japan, D-001210-03-50; Target sequence: AUGUAUUGGCCUGUAUUAG). Cells were analyzed after 24 or 48 h of incubation.

2.3 Western blotting

Proteins were extracted from cells using M-PER mammalian protein extraction reagent (Thermo Fisher Scientific, Inc., Tokyo, Japan, 78503) supplemented with 1X cOmplete Mini protease inhibitor cocktail (Roche Diagnostics, Tokyo, Japan, 04693124001) and 1X PhosSTOP phosphatase inhibitor cocktail (Roche Diagnostics, Tokyo, Japan, 04906845001), separated by 10% sodium dodecyl sulfate (SDS)-polyacrylamide gel electrophoresis (PAGE) and transferred to nitrocellulose membranes. Membranes were blocked with 5% non-fat dry milk and incubated at 4 °C overnight with primary antibody. The following primary antibodies were used: HPV type 16 E6 polyclonal antibody (1:1000; PA5-117355; Thermo Fisher Scientific, Inc., Tokyo, Japan), HPV16/18 E6 (1:200; sc-460; Santa Cruz Biotechnology, Inc., Santa Cruz, CA, USA), HPV16 E7 (1:200; sc-51951; Santa Cruz Biotechnology, Inc., Santa Cruz, CA, USA), HPV18 E7 (1:100; sc-365035; Santa Cruz Biotechnology, Inc., Santa Cruz, CA, USA), p53 (1:1000; sc-126; Santa Cruz Biotechnology, Inc., Santa Cruz, CA, USA), anti-human Retinoblastoma protein (1:1000; 554136; Becton, Dickinson and Company, Franklin Lakes, NJ, USA) and anti-β-tubulin (1:1000; 556321; Becton, Dickinson and Company, Franklin Lakes, NJ, USA). After incubation with goat anti-mouse/rabbit IgG (H + L) HRP-conjugated secondary antibody (1:5000; W4021/W4011; Promega Corporation, Madison, WI, USA), proteins were detected by enhanced chemiluminescence using ECL Select Western Blotting Detection Reagent (GE HealthCare Japan, Tokyo, Japan, RPN2235). The intensity of the target signal was detected using a LAS 500 image analyzer (Cytiva, Tokyo, Japan) and quantified using ImageJ 1.53k software (https://imagej.net/ij/).

2.4 Cell proliferation assay

A total of 2.6×10^5 cells were seeded in 100-mm dishes, incubated overnight and transfected with the siRNAs. After 24 h of incubation, cells were trypsinized, collected and counted using an auto cell counter TC10 (Bio-Rad Laboratories, Inc., Hercules, CA, USA).

TABLE 1. Designations, targets and sequences of the used siRNAs.

siRNA	Target	Name[a]	Sequence[a]
16E6E7	HPV16 E6 & E7	198	5′-GCACACACGUAGACAUUCGdTdT-3′
16E6	HPV16 E6	209	5′-UCCAUAUGCUGUAUGUGAUdTdT-3′
18E6	HPV18 E6	219	5′-CUCUGUGUAUGGAGACACAdTdT-3′
18E6E7	HPV18 E6 & E7	220	5′-UGGAGUUAAUCAUCAACAUdTdT-3′

[a] *The names and sequences of the siRNAs are based on a previous study [15].*
HPV: human papillomavirus; siRNA: small interfering RNA.

2.5 Colony formation assay

A total of 2000 cells were seeded in 6-well plates in triplicate and incubated overnight. Cells were transfected with the siRNAs and cultured in an incubator for 3 weeks. Cells were fixed with 100% methanol and stained with Giemsa, and the colonies consisting of >50 cells in each well were counted manually under a microscope.

2.6 Flow cytometry

A total of 7.8×10^5 cells were seeded in 100-mm dishes, incubated overnight and transfected with the siRNAs. After 24 h of incubation, cells were trypsinized, collected, fixed in ice-cold 70% ethanol and stained with ice-cold propidium iodide (PI)/phosphate-buffered saline (PBS)-Triton/ribonuclease (RNase) A. The cell cycle distribution was analyzed using a FACSVerse flow cytometer (Becton, Dickinson and Company, Franklin Lakes, NJ, USA).

2.7 TdT-mediated dUTP nick-end labeling (TUNEL) assay

A total of 1.2×10^5 cells were seeded on glass coverslips in 6-well plates, incubated overnight and transfected with the siRNAs. After 48 h of incubation, apoptotic cells were analyzed under a fluorescence microscope (Zeiss Axio Imager A1, Zeiss, Oberkochen, BW, Germany) using a DeadEnd Fluorometric TUNEL System (Promega Corporation) according to the manufacturer's instructions.

2.8 Wound healing assay

A total of 2.4×10^5 cells were seeded in 6-well plates and incubated until 90–100% confluent. The cell monolayer was scraped in a straight line with a sterile p1000 pipet tip, and the first images of the scratch at three random points were acquired under a phase-contrast microscope. The cells were transfected with the siRNAs and incubated for 24 h in serum-free medium and the second images were acquired. Distances (μm) between one side of the scratch and the other were measured using ImageJ 1.53k software.

2.9 Transformation assay

Cell transformation was analyzed using a CytoSelect 96-well Cell Transformation Assay Kit (CBA-135; Cell Biolabs, Inc., San Diego, CA, USA) according to the manufacturer's instructions. A total of 3×10^5 cells were seeded in 60-mm dishes, incubated overnight and transfected with the siRNAs. After 24 h of incubation, cells were trypsinized and collected, and cell suspension/agar matrix was prepared. Cell suspension/agar matrix including 2.5×10^3 transfected cells was added into each well of a 96-well sterile microplate containing 50 μL each of agar matrix layer. After 7 days of incubation, anchorage-independent growth was measured based on the absorbance at 570 nm using a plate reader (Sunrise; Tecan Group, Ltd., Männedorf, ZH, Switzerland).

2.10 Microarray and bioinformatics analyses

Total RNAs were extracted using TRIzol reagent (Thermo Fisher Scientific, Inc., Tokyo, Japan, 15596026) from CaSki and HeLa cells transfected with the siRNAs and submitted to Macrogen, Inc., and gene expression profiling was conducted using a SurePrint G3 Human Gene Expression 8 × 60k v3 Microarray (Agilent Technologies, Inc.). Differentially expressed genes (DEGs) were identified using Biometrics Research Branch (BRB)-Array tools v4.6.2 Beta 1 (https://brb.nci.nih.gov/BRB-ArrayTools/) using the class comparison analysis with pairing samples by cell line and setting $p < 0.05$ and $|\log \text{fold change}| \geq 2$ as the cutoff criteria. E7-specific DEGs were extracted using a Venn diagram illustrated by FunRich 3.1.3 software (http://funrich.org/index.html). Gene Ontology (GO) and pathways for the DEGs were identified by functional annotation analyses using the Database for Annotation, Visualization and Integrated Discovery v2022 (DAVID; https://david.ncifcrf.gov/home.jsp; $p < 0.05$; gene count ≥2; Expression Analysis Systematic Explorer (EASE) score ≤0.1) [16] and Metascape v3.5 (https://metascape.org; $p < 0.01$; minimum overlap, 3; minimum enrichment, 1.5) [17]. Protein-Protein Interactions (PPIs) were analyzed using the Search Tool for the Retrieval of Interacting Genes/Proteins v11.5 (STRING; https://string-db.org/; confidence score >0.4) [18] and hub genes, modules and pathway interactions were analyzed using Cytoscape 3.9.1 software (https://cytoscape.org/) [19] using cytoHubba (maximal clique centrality method), Molecular Complex Detection (MCODE) (degree cutoff, 2; node score cutoff, 0.2; k-core, 2; max. depth, 100) and EnrichmentMap (connectivity cutoff of Jaccard similarity, 0.4) tools, respectively. Recurrence-free survival (RFS) in patients with cervical squamous cell carcinoma (n = 174) was compared between groups of patients based on the mRNA expression levels of the DEGs by Kaplan-Meier plotter (https://kmplot.com/analysis/) which utilized gene expression

data and survival information from Gene Expression Omnibus (GEO; https://www.ncbi.nlm.nih.gov/geo/), European Genome-phenome Archive (EGA; https://ega-archive.org/), and The Cancer Genome Atlas (TCGA; https://www.cancer.gov/ccg/research/genome-sequencing/tcga), and *p*-values were calculated by the log-rank test [20].

2.11 Statistical analysis

All data are presented as the mean ± standard deviation (SD) of at least three independent experiments. Differences were compared by one-way analysis of variance (ANOVA) with Tukey's *post-hoc* test or unpaired Student's *t*-test using R version 4.0.5 (https://www.r-project.org/). $p < 0.05$ was considered to indicate a statistically significant difference.

3. Results

3.1 E6/E7 knockdown in CaSki and HeLa cells

In HPV16-positive CaSki cells, both siRNAs 16E6E7 and 16E6 decreased E6 expression and increased p53 expression compared with that in the mock and siRNA NS groups, and siRNA 16E6E7 decreased E7 expression and increased Rb expression compared with that in the mock, siRNA NS and 16E6 groups (Fig. 1A; Table 1). In HPV18-positive HeLa cells, both 18E6 and 18E6E7 decreased E6 expression and increased p53 expression compared with that in the mock and NS groups, and 18E6E7 decreased E7 expression and increased Rb expression compared with that in the mock, NS and 18E6 groups (Fig. 1A; Table 1). Accordingly, comparing the cellular effects of 16E6 with those of mock and NS should indicate mainly the results of HPV16 E6 inhibition, and comparing the cellular effects of 16E6E7 with those of 16E6 should indicate mainly the results of HPV16 E7 inhibition (Table 1). Comparing the cellular effects of 18E6 with those of mock and NS should indicate mainly the results of HPV18 E6 inhibition, and comparing the cellular effects of 18E6E7 with those of 18E6 should indicate mainly the results of HPV18 E7 inhibition (Table 1).

3.2 Effect of knockdown of E6/E7 on cellular proliferation and clonogenicity

Cellular proliferation was significantly inhibited in the 16E6E7 group compared with the 16E6 group in CaSki cells ($p < 0.05$; Fig. 1B,C; Table 2). Colony formation was significantly inhibited in the 16E6E7 group compared with the 16E6 group, and in the 16E6 and 18E6 groups compared with the mock group in CaSki and HeLa cells, respectively ($p < 0.05$, $p < 0.01$ and $p < 0.05$, respectively; Fig. 1D–F; Table 2).

3.3 Effect of knockdown of E6/E7 on the cell cycle and apoptosis

Flow cytometry revealed that the G_0/G_1 cell cycle population was significantly increased in the 16E6E7 group compared with the 16E6 group, and in the 16E6 group compared with the mock group in CaSki cells ($p < 0.01$ and $p < 0.01$, respectively; Fig. 2A–C; Table 2), as well as in the 18E6 group compared with the mock and NS groups, and in the 18E6E7 group compared with the 18E6 group in HeLa cells ($p < 0.01$, $p < 0.05$ and $p < 0.05$, respectively; Fig. 2A–C; Table 2). The sub-G_1 population was not significantly changed in either CaSki or HeLa cells (Fig. 2A,D,E; Table 2). The TUNEL assay showed that 16E6 significantly increased the proportion of apoptotic cells compared with that in the mock group in CaSki cells ($p < 0.05$; Fig. 2F,G; Table 2), and that 18E6 significantly increased the proportion of apoptotic cells compared with that in the mock and NS groups in HeLa cells ($p < 0.01$ and $p < 0.05$, respectively; Fig. 2F–H; Table 2).

3.4 Effect of knockdown of E6/E7 on cell migration and transformation

The wound healing assay revealed that 18E6 significantly inhibited wound healing compared with that in the mock group in HeLa cells ($p < 0.05$; Fig. 3A–C; Table 2). The transformation assay showed that 18E6 significantly inhibited anchorage-independent growth compared with the mock and NS groups in HeLa cells ($p < 0.05$ and $p < 0.05$, respectively; Fig. 3D; Table 2), and that 18E6E7 also significantly inhibited anchorage-independent growth compared with the 18E6 group in HeLa cells ($p < 0.01$; Fig. 3E; Table 2).

TABLE 2. Cellular effects of knocking down E6 or E6/E7 in CaSki and HeLa cell.

Cellular functions	CaSki			HeLa		
	16E6 *vs.* Mock	16E6 *vs.* NS	16E6E7 *vs.* 16E6	18E6 *vs.* Mock	18E6 *vs.* NS	18E6E7 *vs.* 18E6
Cell number	54%	120%	31%[a]	35%	50%	58%
Colony number	44%[b]	102%	12%[a]	20%[a]	29%	58%
G_0/G_1 population	122%[b]	103%	120%[b]	132%[b]	118%[a]	131%[a]
Sub-G_1 population	72%	67%	90%	152%	193%	87%
TUNEL-positive cells	298%[a]	134%	186%	419%[b]	235%[a]	111%
Cell migration	89%	102%	85%	57%[a]	73%	84%
Cell transformation	64%	76%	89%	57%[a]	61%[a]	62%[b]

[a]$p < 0.05$ and [b]$p < 0.01$, one-way ANOVA with Tukey's post-hoc test or unpaired Student's t-test.
NS: Non-specific; TUNEL: TdT-mediated dUTP nick-end labeling.

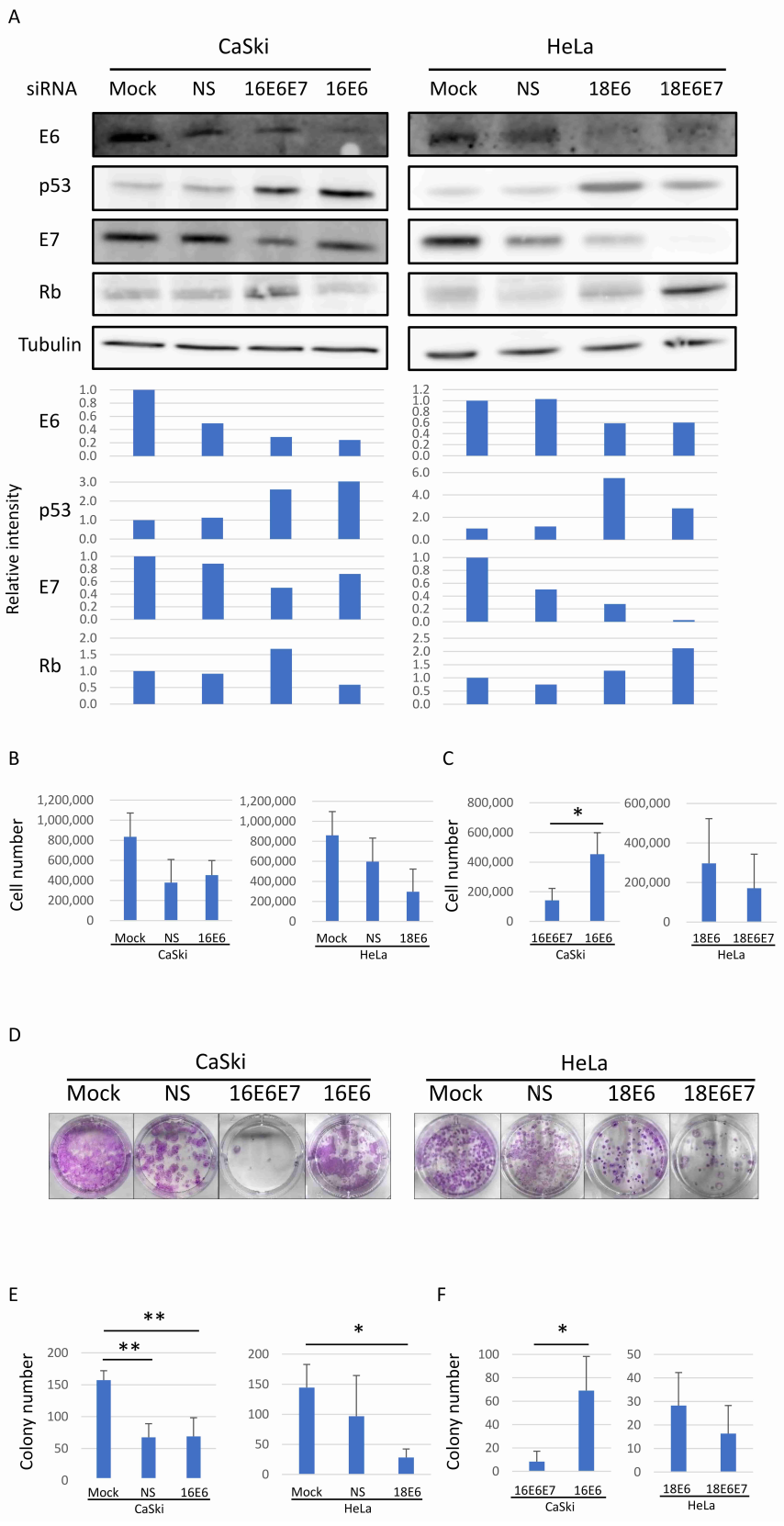

F I G U R E 1. Knockdown of E6/E7 by transfection with mock, NS, 16E6E7, 16E6, 18E6 or 18E6E7 siRNAs in CaSki and HeLa cells (Table 1). (A) Western blotting of E6, E7, p53, Rb and Tubulin, and the relative intensity to Tubulin. (B) Cell numbers following knockdown of E6 based on the cell proliferation assay. (C) Cell numbers following knockdown of E7 based on the cell proliferation assay. (D) Representative well images of the colony formation assay. (E) Colony numbers following knockdown of E6 based on the colony formation assay. (F) Colony numbers following knockdown of E7 based on the colony formation assay. Data are presented as the mean ± SD. Differences were compared by one-way ANOVA with Tukey's *post-hoc* test or unpaired Student's *t*-test. $*p < 0.05$, $**p < 0.01$. NS: Non-specific; siRNA: small interfering RNA.

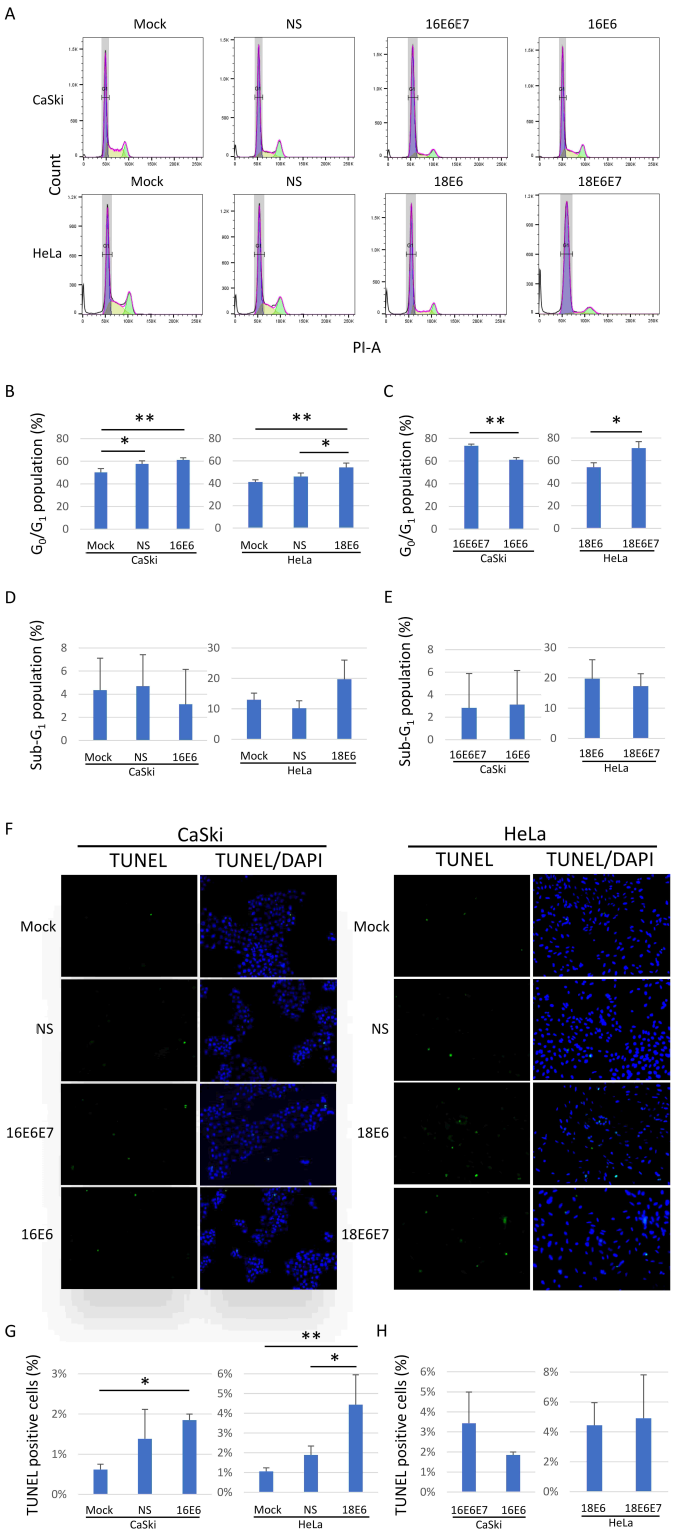

FIGURE 2. Analyses of the cell cycle and apoptosis in CaSki and HeLa cells transfected with mock, NS, 16E6E7, 16E6, 18E6 or 18E6E7 small interfering RNAs (Table 1). (A) Cell cycle distribution. (B) Percentages of cells in the G_0/G_1 phase following knockdown of E6. (C) Percentages of cells in the G_0/G_1 phase following knockdown of E7. (D) Percentages of cells in the sub-G_1 phase following knockdown of E6. (E) Percentages of cells in the sub-G_1 phase following knockdown of E7. (F) Representative images of the TUNEL assay (magnification, ×200). (G) Percentages of TUNEL-positive apoptotic cells following knockdown of E6. (H) Percentages of TUNEL-positive apoptotic cells following knockdown of E7. Data are presented as the mean ± SD. Differences were compared by one-way ANOVA with Tukey's *post-hoc* test or unpaired Student's *t*-test. *$p < 0.05$, **$p < 0.01$. NS: Non-specific; TUNEL: TdT-mediated dUTP nick-end labeling; PI-A: propidium iodide-area; DAPI: 4′,6-diamidino-2-phenylindole.

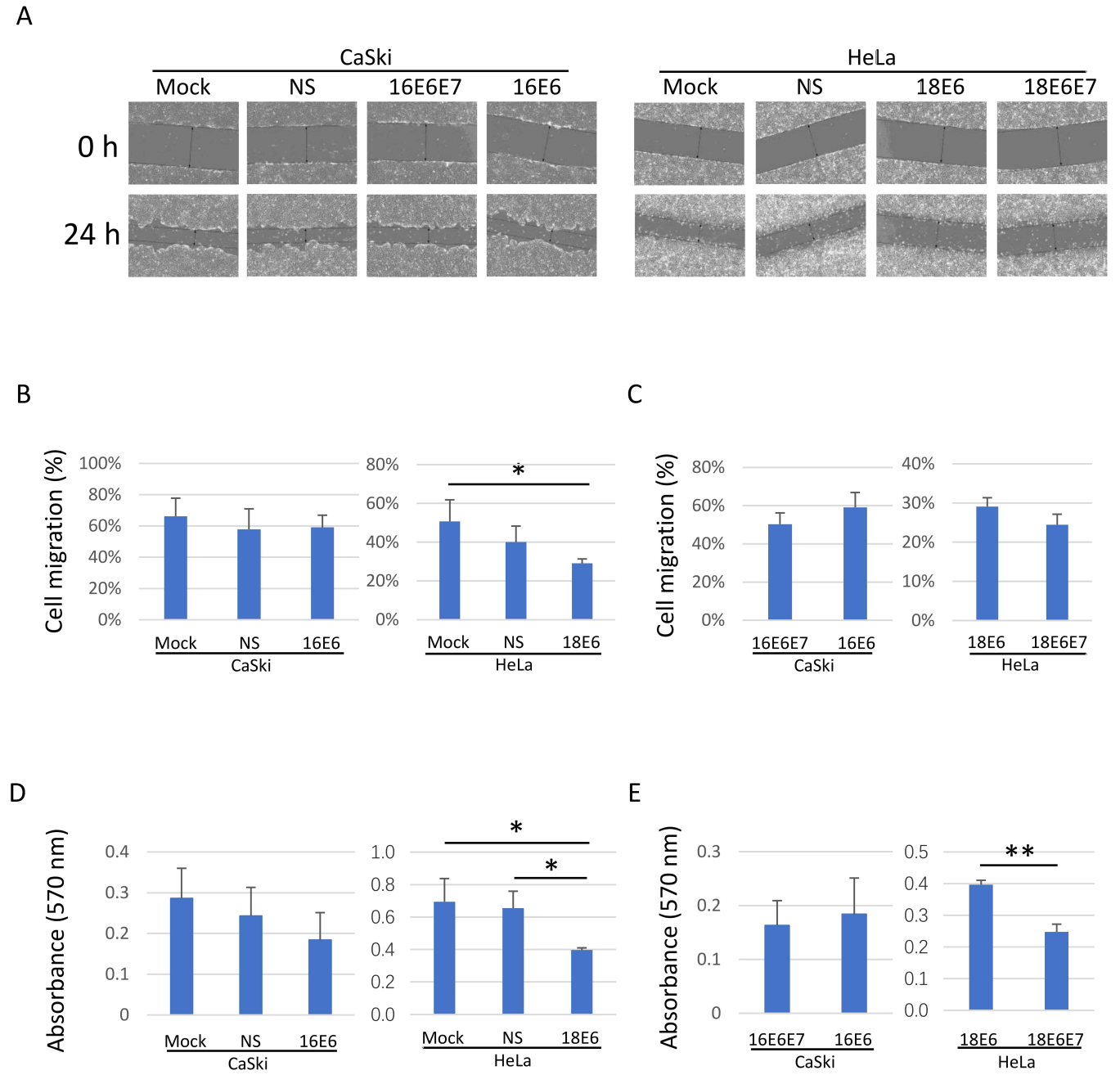

FIGURE 3. Analyses of migration and transformation in CaSki and HeLa cells transfected with mock, NS, 16E6E7, 16E6, 18E6 or 18E6E7 small interfering RNAs (Table 1). (A) Representative images of the wound healing assay (magnification, ×10). (B) Percentages of cell migration following knockdown of E6 based on the wound healing assay. (C) Percentages of cell migration following knockdown of E7 based on the wound healing assay. (D) Anchorage-independent growth (absorbance at 570 nm) following knockdown of E6 based on the transformation assay. (E) Anchorage-independent growth following knockdown of E7 based on the transformation assay. Data are presented as the mean ± SD. Differences were compared by one-way ANOVA with Tukey's *post-hoc* test or unpaired Student's *t*-test. *$p < 0.05$, **$p < 0.01$. NS: Non-specific.

3.5 Microarray and bioinformatics analyses

Microarray analyses were subsequently conducted using RNAs extracted from CaSki and HeLa cells in which E6/E7 were knocked down using the same siRNAs as in the aforementioned experiments. A total of 13,980 genes were analyzed after normalization and filtration. A total of 31 genes were identified as E7-associated DEGs by comparing between 16E6- and 16E6E7-transfected CaSki cells, and between 18E6- and 18E6E7-transfected HeLa cells (Fig. 4A,B). A total of 150 genes were identified as E6-associated DEGs by comparing between NS- and 16E6-transfected CaSki cells, and between NS- and 18E6-transfected HeLa cells (Fig. 4A,B). A total of 222 genes were identified as E6, E7-associated DEGs by comparing between NS- and 16E6E7-transfected CaSki cells, and between NS- and 18E6E7-transfected HeLa cells (Fig. 4A,B). Using FunRich software, the present study further determined the

DEGs identified in both the E7-associated group and the E6, E7-associated group (Fig. 4B). One E6-associated gene was excluded, and finally 15 genes were extracted as the E7-specific DEGs (Fig. 4B; Table 3). Functional annotation analyses of the 15 DEGs using Metascape identified "positive regulation of DNA-binding transcription factor activity", "focal adhesion: phosphatidylinositol 3-kinase (PI3K)-AKT serine/threonine kinase (Akt)-mammalian target of rapamycin (mTOR)-signaling pathway" and "chromatin remodeling" (Fig. 4C,D; Table 4). Functional annotation analyses of the 15 DEGs using DAVID identified "negative regulation of epithelial to mesenchymal transition", "HPV infection", "PI3K-Akt signaling pathway" and "focal adhesion: PI3K-Akt-mTOR-signaling pathway" (Table 5).

The subsequent functional enrichment analysis of the 15 E7-specific DEGs using STRING identified the PPI network shown in Fig. 5A. The Cytoscape software identified one module (Fig. 5B) and the top 8 hub genes (Fig. 5C; Table 6) in the PPI network. The identified pathway interactions for the PPI network based on Cytoscape are shown in Fig. 5D, and the pathways included "G_1 cell cycle arrest", "focal adhesion: PI3K-Akt-mTOR-signaling", "formation of senescence-associated heterochromatin foci (SAHF)" and "apoptotic signaling pathway".

The prognosis of patients with cervical squamous cell carcinoma was further analyzed according to the mRNA expression levels of the E7-specific DEGs using the web-based survival analysis tool Kaplan-Meier plotter. High expression levels of aldo-keto reductase family 1 member B10 (*AKR1B10*), family with sequence similarity 78 member A (*FAM78A*) and AHNAK nucleoprotein 2 (*AHNAK2*) ($p = 0.00095$, $p = 0.0034$ and $p = 0.014$; Fig. 6) were significantly associated with improved RFS, whereas high expression levels of forkhead box A1 (*FOXA1*), SMAD family member 9 (*SMAD9*) and plastin 1 (*PLS1*) were significantly associated with worse RFS ($p = 0.0014$, $p = 0.027$ and $p = 0.039$; Fig. 6).

TABLE 3. E7-specific DEGs identified by the microarray analysis in CaSki and HeLa cells.

Gene symbol	Description	Fold difference of geometric mean gene expressions	Parametric *p*-value[a]	Log-ratio of normalized gene expressions	
				CaSki	HeLa
SLC44A1	solute carrier family 44 member 1	3.07	<0.001	1.52	1.71
AKR1B10	aldo-keto reductase family 1 member B10	0.43	<0.001	−1.11	−1.34
RTKN2	rhotekin 2	2.12	<0.001	1.07	1.09
NFE2	nuclear factor, erythroid 2	0.50	0.001	−1.14	−0.88
ARL5B	ADP ribosylation factor like GTPase 5B	2.11	0.003	0.75	1.40
FOXA1	forkhead box A1	2.20	0.005	0.68	1.60
PPP2R2B	protein phosphatase 2 regulatory subunit Bbeta	2.54	0.010	0.62	2.07
SMAD9	SMAD family member 9	2.49	0.011	0.58	2.05
FAM78A	family with sequence similarity 78 member A	0.48	0.011	−0.51	−1.60
PTEN	phosphatase and tensin homolog	2.37	0.012	0.55	1.95
GALNT1	polypeptide N-acetylgalactosaminyltransferase 1	2.53	0.012	0.57	2.11
H1-1	H1.1 linker histone, cluster member	2.14	0.013	0.41	1.78
PLS1	plastin 1	2.33	0.026	0.35	2.09
CCNE1	cyclin E1	2.06	0.027	0.32	1.78
AHNAK2	AHNAK nucleoprotein 2	0.49	0.030	−0.28	−1.75

[a] *Paired t-test with random variance model.*

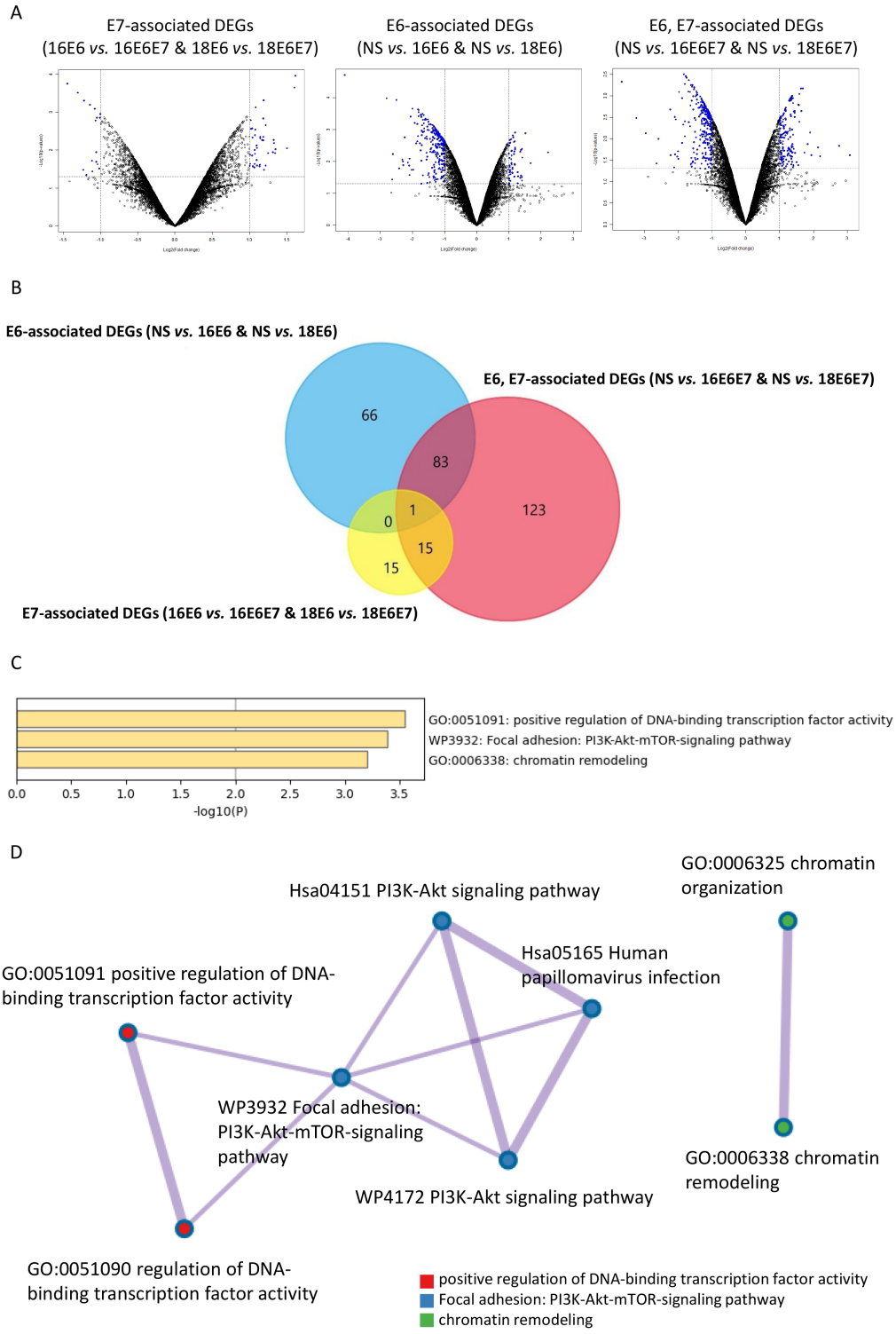

FIGURE 4. Microarray analysis and functional annotation using RNAs from small interfering RNA-transfected cells. (A) Volcano plots of E7-associated DEGs (comparing 16E6- *vs.* 16E6E7-transfected CaSki cells and 18E6- *vs.* 18E6E7-transfected HeLa cells), E6-associated DEGs (comparing NS- *vs.* 16E6-transfected CaSki cells and NS- *vs.* 18E6-transfected HeLa cells) and E6, E7-associated DEGs (comparing NS- *vs.* 16E6E7-transfected CaSki cells and NS- *vs.* 18E6E7-transfected HeLa cells). *p*-values ($-\log_{10}$) are plotted against FC ($\log_2$). Upregulated ($\log_2 FC \geq 1$ and $p < 0.05$) and downregulated ($\log_2 FC \leq -1$ and $p < 0.05$) DEGs are denoted by blue nodes. (B) Venn diagram showing the overlap among E7-associated, E6-associated and E6, E7-associated DEGs. (C) Functional annotation using Metascape of the 15 E7-specific DEGs extracted from the Venn diagram. (D) Enriched ontology clusters based on Metascape analysis of the 15 E7-specific DEGs. FC: fold change. DEGs: differentially expressed genes; NS: Non-specific; GO: Gene Ontology; PI3K: phosphatidylinositol 3-kinase; Akt: AKT serine/threonine kinase; mTOR: mammalian target of rapamycin.

TABLE 4. Functional annotation of the E7-specific DEGs by Metascape.

Group ID	Category	Term	Description	Log_{10} *p*-value	Symbols
1_Summary	GO Biological Processes	GO:0051091	Positive regulation of DNA-binding transcription factor activity	−3.55	*FOXA1*, *PTEN*, *RTKN2*
1_Member	GO Biological Processes	GO:0051091	Positive regulation of DNA-binding transcription factor activity	−3.55	*FOXA1*, P*TEN*, *RTKN2*
1_Member	GO Biological Processes	GO:0051090	Regulation of DNA-binding transcription factor activity	−2.87	*FOXA1*, P*TEN*, *RTKN2*
2_Summary	WikiPathways	WP3932	Focal adhesion: PI3K-Akt-mTOR-signaling pathway	−3.38	*FOXA1*, *PPP2R2B*, *PTEN*, *CCNE1*
2_Member	WikiPathways	WP3932	Focal adhesion: PI3K-Akt-mTOR-signaling pathway	−3.38	*FOXA1*, *PPP2R2B*, *PTEN*
2_Member	KEGG Pathway	hsa05165	Human papillomavirus infection	−3.27	*CCNE1*, *PPP2R2B*, *PTEN*
2_Member	WikiPathways	WP4172	PI3K-Akt signaling pathway	−3.24	*CCNE1*, *PPP2R2B*, *PTEN*
2_Member	KEGG Pathway	hsa04151	PI3K-Akt signaling pathway	−3.18	*CCNE1*, *PPP2R2B*, *PTEN*
3_Summary	GO Biological Processes	GO:0006338	Chromatin remodeling	−3.20	*H1-1*, *FOXA1*, *NFE2*
3_Member	GO Biological Processes	GO:0006338	Chromatin remodeling	−3.20	*H1-1*, *FOXA1*, *NFE2*
3_Member	GO Biological Processes	GO:0006325	Chromatin organization	−2.51	*H1-1*, *FOXA1*, *NFE2*

GO: Gene Ontology; FOXA1: forkhead box A1; PTEN: phosphatase and tensin homolog; RTKN2: rhotekin 2; PPP2R2B: protein phosphatase 2 regulatory subunit Bbeta; CCNE1: cyclin E1; H1-1: H1.1 linker histone, cluster member; NFE2: nuclear factor, erythroid 2; PI3K: phosphatidylinositol 3-kinase; Akt: AKT serine/threonine kinase; mTOR: mammalian target of rapamycin; ID: identifier.

TABLE 5. Functional annotation of the E7-specific DEGs by DAVID.

Term	Description	Count	%	*p*-value	Genes	List total	Pop hits	Pop total	Fold enrichment	Bonferroni	Benjamini	FDR
GO:0010719	Negative regulation of epithelial to mesenchymal transition	2	13	0.025	*FOXA1*, *PTEN*	14	38	19308	72.6	1	1	1
hsa05165	Human papillomavirus infection	3	20	0.030	*PPP2R2B*, *CCNE1*, *PTEN*	8	331	8164	9.25	0.81	0.88	0.88
hsa04151	PI3K-Akt signaling pathway	3	20	0.034	*PPP2R2B*, *CCNE1*, *PTEN*	8	354	8164	8.65	0.85	0.88	0.88
WP3932	Focal adhesion: PI3K-Akt-mTOR-signaling pathway	3	20	0.035	*FOXA1*, *PPP2R2B*, *PTEN*	9	302	7879	8.70	0.92	1	1
WP4172	PI3K-Akt signaling pathway	3	20	0.043	*PPP2R2B*, *CCNE1*, *PTEN*	9	339	7879	7.75	0.96	1	1

FDR, false discovery rate; GO: Gene Ontology; FOXA1: forkhead box A1; PTEN: phosphatase and tensin homolog; RTKN2: rhotekin 2; PPP2R2B: protein phosphatase 2 regulatory subunit Bbeta; CCNE1: cyclin E1; PI3K: phosphatidylinositol 3-kinase; Akt: AKT serine/threonine kinase; mTOR: mammalian target of rapamycin.

TABLE 6. Hub genes in the PPI network of the E7-specific DEGs.

Rank	Name	Gene	Score
1	9606.ENSP00000269305	*TP53*	56
2	9606.ENSP00000262643	*CCNE1*	54
2	9606.ENSP00000266970	*CDK2*	54
4	9606.ENSP00000361021	*PTEN*	51
5	9606.ENSP00000281708	*FBXW7*	24
5	9606.ENSP00000228872	*CDKN1B*	24
7	9606.ENSP00000244573	*H1-1*	6
8	9606.ENSP00000250448	*FOXA1*	2

FOXA1: forkhead box A1; PTEN: phosphatase and tensin homolog; CCNE1: cyclin E1; H1-1: H1.1 linker histone, cluster member; TP53: tumor protein p53; CDK2: cyclin dependent kinase 2; FBXW7: F-box and WD repeat domain containing 7; CDKN1B: cyclin dependent kinase inhibitor 1B.

4. Discussion

Our previous study on separately analyzing *E6*/*E7* mRNAs in liquid-based cytology samples indicated that the presence of *E7* mRNAs correlated with progression from low-grade cervical intraepithelial neoplasia (CIN) to invasive cancer by contrast with the presence of *E6* mRNA, and that the presence of both *E6* and *E7* mRNAs was associated with upgraded abnormal cytology in the followed-up patients with CIN1–2 in contrast to the presence of *E6* mRNA [14]. These findings are in line with multiple reports, where the positive rate of E7 mRNA/protein expression increased with CIN grade [10–12], and *E7* mRNA predicted progression to high-grade squamous intraepithelial lesion/CIN2+ [13]. Furthermore, *in vitro* studies have revealed that the expression of E7 by itself could immortalize human keratinocytes at a low frequency but E6 had no such activity, and that the combined expression of E6 and E7 could efficiently immortalize most types of primary cells [21, 22]. Furthermore, in a transgenic mouse model, E7 alone, but not E6 alone, was sufficient to induce high-grade CIN and invasive cancer, and E6 addition resulted in larger and more extensive tumors [23]. Taken together, accumulating evidence suggests that E7 may contribute more closely to cervical carcinogenesis than E6. Although numerous molecules and pathways downstream of E6 and E7 have been identified, the precise mechanism whereby E7 exhibits stronger involvement in cervical carcinogenesis than E6 is yet to be fully clarified, and this was explored in the present study.

The cellular effects of knocking down E6/E7 in HPV-positive CaSki and HeLa cells were evaluated, as summarized in Table 2. The cell proliferation and colony formation assays suggested that knockdown of E7 and knockdown of E6 both inhibited cellular proliferation and/or clonogenicity (Fig. 1B,D; Table 2). Flow cytometry suggested that knockdown of E7 and knockdown of E6 both induced G_1 cell cycle arrest (Fig. 2A,B; Table 2). The TUNEL assay suggested that knockdown of E6 induced apoptosis (Fig. 2E; Table 2). The wound healing assay suggested that knockdown of E6 inhibited cell migration (Fig. 3B; Table 2). The transformation assay suggested that knockdown of E7 and knockdown of E6 both inhibited cellular transformation (Fig. 3C; Table 2). These observed differential cellular effects of knockdown of E6 or E7 were consistent with published findings [24].

Flow cytometry exhibited that knockdown of E7 induced G_1 cell cycle arrest (Fig. 2B; Table 2), and the pathway interaction for the E7-specific PPI network using Cytoscape revealed that G_1 cell cycle arrest was the most significant and pivotal pathway (Fig. 5D). These findings suggest that G_1 cell cycle arrest may be the most important E7-specific carcinogenic pathway. Besides G_1 cell cycle arrest, the functional annotations based on Metascape and DAVID analyses both included "focal adhesion: PI3K-Akt-mTOR-signaling pathway", those of Metascape analysis included "chromatin remodeling", and those of DAVID analysis included "negative regulation of epithelial to mesenchymal transition" (Tables 4 and 5). All of these pathways reportedly contribute to cellular transformation [25–28]. The transformation assay demonstrated that knockdown of E7 inhibited cellular transformation (Fig. 3E; Table 2), suggesting that these three pathways may contribute to the E7-specifc cervical carcinogenesis via cellular transformation. Additionally, these pathways including G_1 cell cycle arrest as well as PI3K-Akt-mTOR-signaling pathway are considered to provide the ideal molecular targets for more effective treatment of cervical cancer.

The survival analyses of groups of patients based on the expression levels of the E7-specific DEGs showed that *AKR1B10*, *FAM78A* and *AHNAK2* were associated with improved prognosis, while *FOXA1*, *SMAD9* and *PLS1* were associated with worse prognosis in cervical cancer (Fig. 6). These oncogenic or tumor-suppressive prognostic significances were consistent with the fold differences of the gene expression levels in the microarray analyses (Table 3). These findings are further supported by published findings. AKR1B10, a member of the aldo/keto reductase superfamily, catalyzes the conversion of retinal to retinol, and thus, counteracts the formation of retinoic acid, which is involved in cell proliferation and differentiation [29]. High expression levels of *FAM78A* are associated with improved overall survival in pancreatic adenocarcinoma [30]. Knockdown of AHNAK2, a large nucleoprotein, has been reported to lead to radioresistance in esophageal squamous cell carcinoma cells [31]. Knockdown of FOXA1, the founding member of the FOX family of transcription factors [32], reverses chemoresistance by suppressing cell proliferation, migration and epithelial-mesenchymal transition, and high *FOXA1* expression is associated with chemoresistant cells and worse patient survival in lung adenocarcinoma [33]. A single nucleotide polymorphism in *SMAD9*, a member of the SMAD family that transduces signals from the transforming growth factor (TGF)-β pathway, is associated with unfavorable survival in non-small cell lung cancer after radiotherapy [34]. PLS1, a member of the actin-binding protein family, has been implicated to promote metastasis of colorectal cancer [35]. Therefore, it is suggested that these DEGs may serve as useful biomarkers for the prognosis of cervical cancer.

Tumor protein p53 (*TP53*) is one of the most mutated hu-

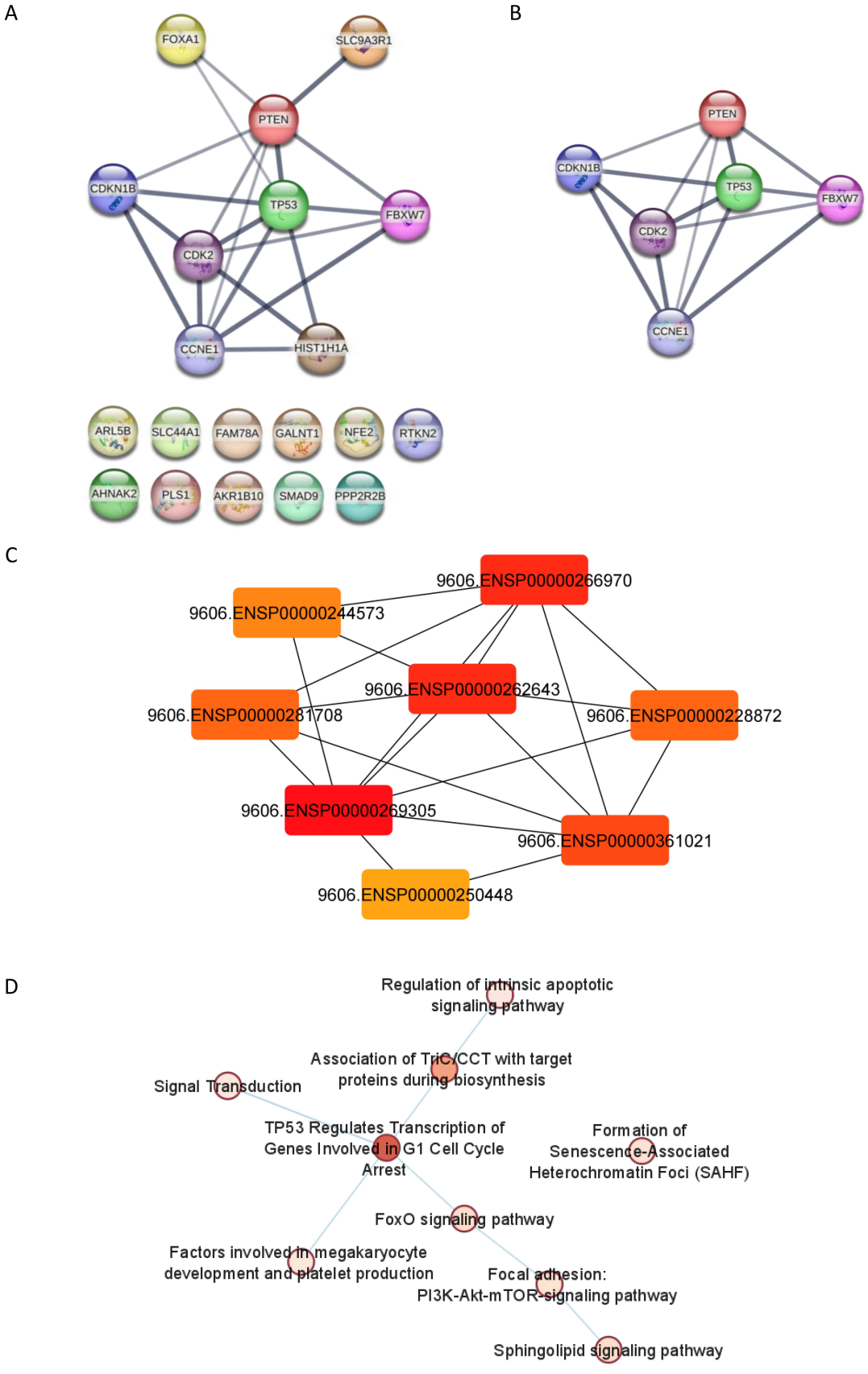

FIGURE 5. Analyses of the PPI network, module, hub genes and pathway interactions of the 15 E7-specific DEGs by STRING and Cytoscape. (A) PPI network generated using STRING. (B) Module of the PPI network. (C) Top 8 hub genes of the PPI network based on the maximal clique centrality method. (D) Pathway interactions of the PPI network. PPI: Protein-Protein Interaction; DEGs: differentially expressed genes; STRING: Search Tool for the Retrieval of Interacting Genes/Proteins.

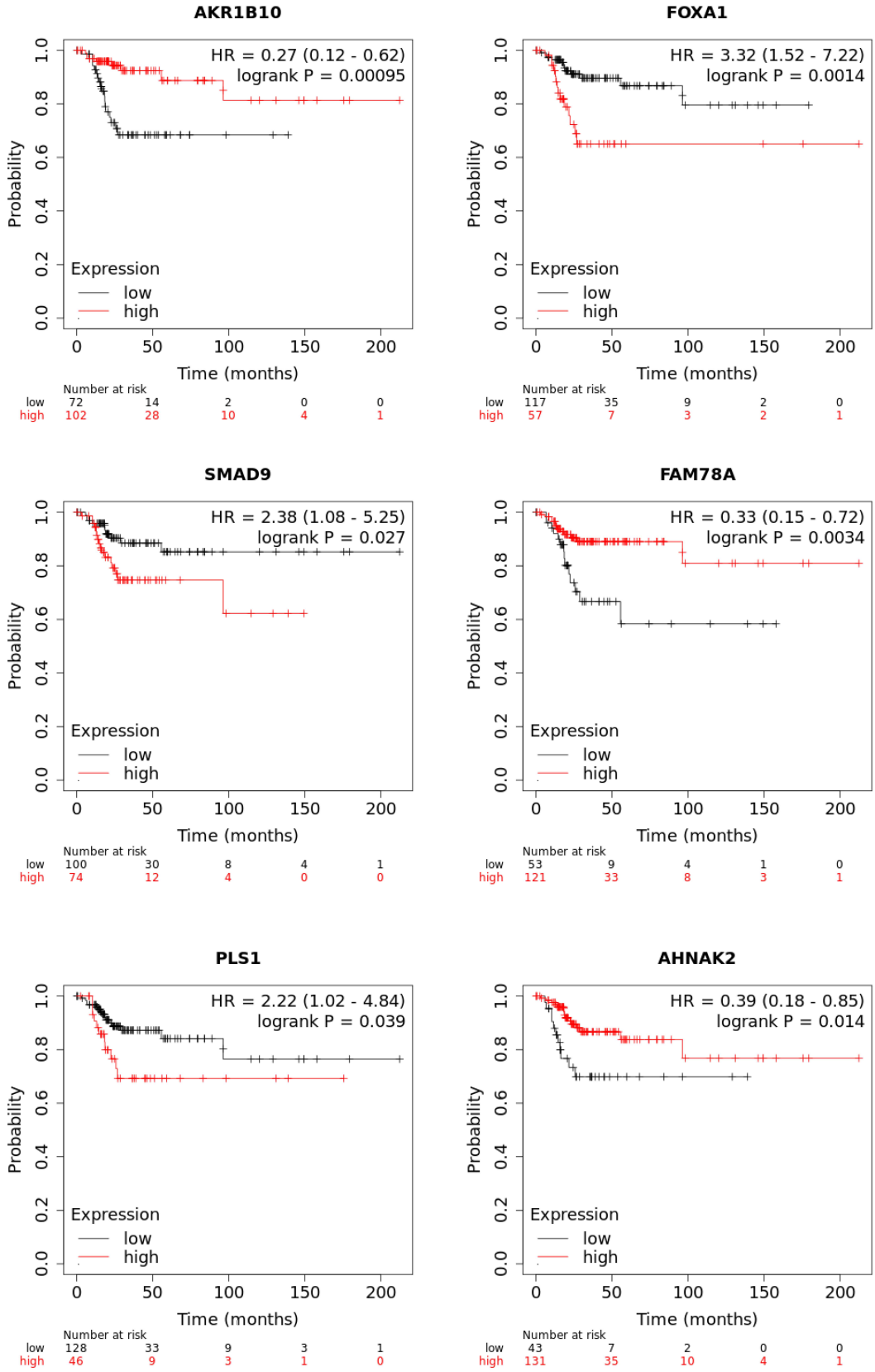

FIGURE 6. Recurrence-free survival curves obtained utilizing Kaplan-Meier plotter in patients with cervical squamous cell carcinoma (n = 174) according to the mRNA expression levels of the E7-specific DEGs. HR: hazard ratio; *AKR1B10*: aldo-keto reductase family 1 member B10; *FOXA1*: forkhead box A1; *SMAD9*: SMAD family member 9; *FAM78A*: family with sequence similarity 78 member A; *PLS1*: plastin 1; *AHNAK2*: AHNAK nucleoprotein 2.

man gene involved in numerous cellular functions [3], and is known to be involved even in Rb-mediated G_1/S cell cycle checkpoint through cyclin dependent kinase inhibitor 1A/p21 [36]. Therefore, the finding that *TP53* ranked as the most significant hub gene of the E7-specific PPI network should be reasonable (Table 6). Although *Rb* was not among the top 8 hub genes of the E7-specific PPI network, cyclin E1 and cyclin dependent kinase 2 (*CDK2*), ranked as the second and third hub genes (Table 6), are also known to be involved in the Rb-mediated G_1/S cell cycle checkpoint [37]. Phosphatase and tensin homolog (*PTEN*) and cyclin dependent kinase inhibitor 1B/p27, ranked as the fourth and sixth hub genes (Table 6), are also known to be involved in the Rb-mediated G_1/S checkpoint through the PI3K/Akt signaling pathway [38, 39]. Additionally, E7 reportedly interacts with numerous proteins other than Rb, and E6 interacts with numerous proteins other than p53 [24], supporting the present results on the hub genes in the PPI network of the E7-specific DEGs.

This study has some limitations. First, the siRNA experiments were based on transient transfection, not stable transfection. Second, the data on E7-specific DEGs were extracted by comparing results indirectly from siRNA experiments. Third, NS siRNA decreased E6 levels in both cell lines, and decreased E7 levels in HeLa cells, compared with those in the mock group. As possible consequences, NS siRNA significantly inhibited colony formation and increased the G_0/G_1 cell cycle population in CaSki cells compared with those in the mock group. Although other NS siRNAs were tested, the results were similar. Therefore, the significant cellular effects of knockdown of E6 were evaluated by comparing with mock as well as NS. Lastly, reverse transcription-polymerase chain reaction (PCR) experiments using the same siRNAs are necessary to validate the DEGs and hub genes to be E7-specific. Nevertheless, our reasonable findings in view of the previous multiple publications support the significance of the current study. Further exploring the E7-specific pathways *in vivo* as well as across other types of HR-HPVs will provide beneficial information for the management of cervical neoplastic diseases.

5. Conclusions

The present study explored the precise E7-specific pathways involved in cervical carcinogenesis. The current findings suggest that the identified DEGs contribute to the E7-specific cervical carcinogenesis by cooperating through the multiple pathways, providing significant implications for novel targets and biomarkers for more efficient prophylactic and therapeutic strategies for cervical cancer.

AVAILABILITY OF DATA AND MATERIALS

The data generated in this study may be requested from the corresponding author.

AUTHOR CONTRIBUTIONS

NQ—conducted the experiments; acquired data and drafted the manuscript. TM—conceptualized the study; conducted statistical analysis and edited the manuscript. KF, AsS, HI, YT, AyS, NT, AA, SN and TS—interpreted data and critically reviewed the manuscript. AA—acquired funding. TS—supervised the study. NQ and TM—confirm the authenticity of all the raw data. All authors read and approved the final manuscript.

ETHICS APPROVAL AND CONSENT TO PARTICIPATE

Not applicable.

ACKNOWLEDGMENT

Not applicable.

FUNDING

This study was partially supported by a Grant-in-Aid for Scientific Research (grant no. 21K09464) from the Ministry of Education, Culture, Sports, Science and Technology, Tokyo, Japan.

CONFLICT OF INTEREST

The authors declare no conflict of interest.

REFERENCES

[1] Anderson DM, Lee J, Elkas JC. Cervical and vaginal cancer. In Berek JS, Berek DL (eds.) Berek & Novak's gynecology (pp. 1039). 16th edn. Wolters Kluwer: Torrance. 2020.

[2] Hatano T, Sano D, Takahashi H, Oridate N. Pathogenic role of immune evasion and integration of human papillomavirus in oropharyngeal cancer. Microorganisms. 2021; 9: 891.

[3] Patil MR, Bihari A. A comprehensive study of p53 protein. Journal of Cellular Biochemistry. 2022; 123: 1891–1937.

[4] Martínez-Sánchez M, Hernandez-Monge J, Rangel M, Olivares-Illana V. Retinoblastoma: from discovery to clinical management. The FEBS Journal. 2022; 289: 4371–4382.

[5] Rasi Bonab F, Baghbanzadeh A, Ghaseminia M, Bolandi N, Mokhtarzadeh A, Amini M, *et al*. Molecular pathways in the development of HPV-induced cervical cancer. EXCLI Journal. 2021; 20: 320–337.

[6] Bhattacharjee R, Das SS, Biswal SS, Nath A, Das D, Basu A, *et al*. Mechanistic role of HPV-associated early proteins in cervical cancer: molecular pathways and targeted therapeutic strategies. Critical Reviews in Oncology/Hematology. 2022; 174: 103675.

[7] Muñoz N, Bosch FX, de Sanjosé S, Herrero R, Castellsagué X, Shah KV, *et al*. Epidemiologic classification of human papillomavirus types associated with cervical cancer. The New England Journal of Medicine. 2003; 348: 518–527.

[8] Graham SV. The human papillomavirus replication cycle, and its links to cancer progression: a comprehensive review. Clinical Science. 2017; 131: 2201–2221.

[9] Zheng Y, Li X, Jiao Y, Wu C. High-risk human papillomavirus oncogenic E6/E7 mRNAs splicing regulation. Frontiers in Cellular and Infection Microbiology. 2022; 12: 929666.

[10] Kong L, Xiao X, Lou H, Liu P, Song S, Liu M, *et al*. Analysis of the role of the human papillomavirus 16/18 E7 protein assay in screening

for cervical intraepithelial neoplasia: a case control study. BMC Cancer. 2020; 20: 999.

[11] Nakagawa S, Yoshikawa H, Yasugi T, Kimura M, Kawana K, Matsumoto K, *et al*. Ubiquitous presence of E6 and E7 transcripts in human papillomavirus-positive cervical carcinomas regardless of its type. Journal of Medical Virology. 2000; 62: 251–258.

[12] Sotlar K, Stubner A, Diemer D, Menton S, Menton M, Dietz K, *et al*. Detection of high-risk human papillomavirus E6 and E7 oncogene transcripts in cervical scrapes by nested RT-polymerase chain reaction. Journal of Medical Virology. 2004; 74: 107–116.

[13] Martí C, Marimón L, Glickman A, Henere C, Saco A, Rakislova N, *et al*. Usefulness of E7 mRNA in HPV16-positive women to predict the risk of progression to HSIL/CIN2. Diagnostics. 2021; 11: 1634.

[14] Liu S, Minaguchi T, Lachkar B, Zhang S, Xu C, Tenjimbayashi Y, *et al*. Separate analysis of human papillomavirus E6 and E7 messenger RNAs to predict cervical neoplasia progression. PLOS ONE. 2018; 13: e0193061.

[15] Tang S, Tao M, McCoy JP III, Zheng ZM. The E7 oncoprotein is translated from spliced E6*I transcripts in high-risk human papillomavirus type 16- or type 18-positive cervical cancer cell lines via translation reinitiation. Journal of Virology. 2006; 80: 4249–4263.

[16] Sherman BT, Hao M, Qiu J, Jiao X, Baseler MW, Lane HC, *et al*. DAVID: a web server for functional enrichment analysis and functional annotation of gene lists (2021 update). Nucleic Acids Research. 2022; 50: W216–W221.

[17] Zhou Y, Zhou B, Pache L, Chang M, Khodabakhshi AH, Tanaseichuk O, *et al*. Metascape provides a biologist-oriented resource for the analysis of systems-level datasets. Nature Communications. 2019; 10: 1523.

[18] Szklarczyk D, Kirsch R, Koutrouli M, Nastou K, Mehryary F, Hachilif R, *et al*. The STRING database in 2023: protein-protein association networks and functional enrichment analyses for any sequenced genome of interest. Nucleic Acids Research. 2023; 51: D638–D646.

[19] Shannon P, Markiel A, Ozier O, Baliga NS, Wang JT, Ramage D, *et al*. Cytoscape: a software environment for integrated models of biomolecular interaction networks. Genome Research. 2003; 13: 2498–2504.

[20] Győrffy B. Integrated analysis of public datasets for the discovery and validation of survival-associated genes in solid tumors. Innovation. 2024; 5: 100625.

[21] Hawley-Nelson P, Vousden KH, Hubbert NL, Lowy DR, Schiller JT. HPV16 E6 and E7 proteins cooperate to immortalize human foreskin keratinocytes. The EMBO Journal. 1989; 8: 3905–3910.

[22] Münger K, Phelps WC, Bubb V, Howley PM, Schlegel R. The E6 and E7 genes of the human papillomavirus type 16 together are necessary and sufficient for transformation of primary human keratinocytes. Journal of Virology. 1989; 63: 4417–4421.

[23] Riley RR, Duensing S, Brake T, Münger K, Lambert PF, Arbeit JM. Dissection of human papillomavirus E6 and E7 function in transgenic mouse models of cervical carcinogenesis. Cancer Research. 2003; 63: 4862–4871.

[24] Scarth JA, Patterson MR, Morgan EL, Macdonald A. The human papillomavirus oncoproteins: a review of the host pathways targeted on the road to transformation. Journal of General Virology. 2021; 102: 001540.

[25] Jia W, Feng YI, Sanders AJ, Davies EL, Jiang WG. Phosphoinositide-3-Kinase Enhancers, PIKEs: their biological functions and roles in cancer. Anticancer Research. 2016; 36: 1103–1109.

[26] Soshnev AA, Allis CD, Cesarman E, Melnick AM. Histone H1 mutations in lymphoma: a link(er) between chromatin organization, developmental reprogramming, and cancer. Cancer Research. 2021; 81: 6061–6070.

[27] Katoh M, Igarashi M, Fukuda H, Nakagama H, Katoh M. Cancer genetics and genomics of human FOX family genes. Cancer Letters. 2013; 328: 198–206.

[28] Bersaas A, Arnoldussen YJ, Sjøberg M, Haugen A, Mollerup S. Epithelial-mesenchymal transition and FOXA genes during tobacco smoke carcinogen induced transformation of human bronchial epithelial cells. Toxicology in Vitro. 2016; 35: 55–65.

[29] Rizner TL. Enzymes of the AKR1B and AKR1C subfamilies and uterine diseases. Frontiers in Pharmacology. 2012; 3: 34.

[30] Liao X, Huang K, Huang R, Liu X, Han C, Yu L, *et al*. Genome-scale analysis to identify prognostic markers in patients with early-stage pancreatic ductal adenocarcinoma after pancreaticoduodenectomy. OncoTargets and Therapy. 2017; 10: 4493–4506.

[31] Hou Q, Jiang Z, Li Z, Jiang M. Identification and functional validation of radioresistance-related genes AHNAK2 and EVPL in esophageal squamous cell carcinoma by exome and transcriptome sequencing analyses. OncoTargets and Therapy. 2021; 14: 1131–1145.

[32] Bernardo GM, Keri RA. FOXA1: a transcription factor with parallel functions in development and cancer. Bioscience Reports. 2012; 32: 113–130.

[33] Chen D, Wang R, Yu C, Cao F, Zhang X, Yan F, *et al*. FOX-A1 contributes to acquisition of chemoresistance in human lung adenocarcinoma via transactivation of SOX5. EBioMedicine. 2019; 44: 150–161.

[34] Zhang H, Wang W, Pi W, Bi N, DesRosiers C, Kong F, *et al*. Genetic variations in the transforming growth factor-β1 pathway may improve predictive power for overall survival in non-small cell lung cancer. Frontiers in Oncology. 2021; 11: 599719.

[35] Zhang T, Wang Z, Liu Y, Huo Y, Liu H, Xu C, *et al*. Plastin 1 drives metastasis of colorectal cancer through the IQGAP1/Rac1/ERK pathway. Cancer Science. 2020; 111: 2861–2871.

[36] Slebos RJ, Lee MH, Plunkett BS, Kessis TD, Williams BO, Jacks T, *et al*. p53-dependent G1 arrest involves pRB-related proteins and is disrupted by the human papillomavirus 16 E7 oncoprotein. Proceedings of the National Academy of Sciences of the United States of America. 1994; 91: 5320–5324.

[37] Zhang HS, Gavin M, Dahiya A, Postigo AA, Ma D, Luo RX, *et al*. Exit from G1 and S phase of the cell cycle is regulated by repressor complexes containing HDAC-Rb-hSWI/SNF and Rb-hSWI/SNF. Cell. 2000; 101: 79–89.

[38] Paramio JM, Navarro M, Segrelles C, Gómez-Casero E, Jorcano JL. PTEN tumour suppressor is linked to the cell cycle control through the retinoblastoma protein. Oncogene. 1999; 18: 7462–7468.

[39] Busse D, Doughty RS, Ramsey TT, Russell WE, Price JO, Flanagan WM, *et al*. Reversible G (1) arrest induced by inhibition of the epidermal growth factor receptor tyrosine kinase requires up-regulation of p27(KIP1) independent of MAPK activity. Journal of Biological Chemistry. 2000; 275: 6987–6995.

How to cite this article: Nan Qi, Takeo Minaguchi, Kaoru Fujieda, Asami Suto, Hiroya Itagaki, Yuri Tenjimbayashi, *et al*. Functional, microarray and bioinformatics analyses of human papillomavirus E7-specific pathways in cervical carcinogenesis. European Journal of Gynaecological Oncology. 2025; 46(5): 8-23. doi: 10.22514/ejgo.2025.061.